Adaptive Polymeric Coatings with Self-Reporting and Self-Healing Dual Functions from Porous Core-shell Nanostructures

Jun-Peng Wang,[1,2] Jun-Kuo Wang,[3] Qiong Zhou,[3] Zhan Li,[1] Yongsheng Han,[1]Yan Song,[1] Shuo Yang,[1]Tao Qi*[1,2] Helmuth Möhwald,[4] Dmitry Shchukin,[5] and Guo Liang Li*[1,2]

[1]Institute of Process Engineering, Chinese Academy of Sciences, Beijing, 100190, P. R. China

[2]University of Chinese Academy of Sciences, Beijing, 100049, P. R. China

[3]Department of Materials Science and Engineering, China University of Petroleum, Beijing 102249, P. R. China

[4]Max Planck Institute of Colloids and Interfaces, Wissenschaftspark Golm, 14476 Potsdam, Germany

[5]Stephenson Institute for Renewable Energy, Department of Chemistry, University of Liverpool, Crown Street, Liverpool, L69 7ZD, United Kingdom

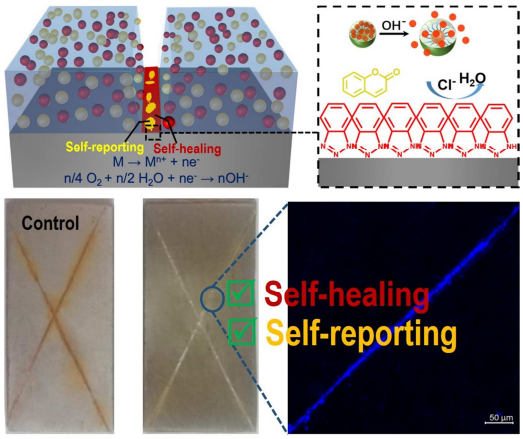

Corresponding author: Prof. Guo Liang Li and Prof. Tao Qi

Tel:+86-10-82544934

E-mail address: glli@ipe.ac.cn (G. Li); tqi@ipe.ac.cn (T. Qi)

ABSTRACT

In addition to autonomous self-healing ability of smart materials developed to extend life-cycle control, it is essential for intentional intervention in many instances in conducting regular maintenance thus making sense of self-reporting of early cracks/damage of materials. The present work introduces an intelligent pH-responsive coating based on the designed poly(divinylbenzene)-*graft*-poly(divinylbenzene-*co*-methacrylic acid) (PDVB-*graft*-P(DVB-*co*-AA)) core-shell microspheres as smart microspheres. As the key component, the synthesized PDVB-*graft*-P(DVB-*co*-AA) core-shell microspheres are porous and pH-responsive, respective. The porosity allows for encapsulation of corrosion inhibitor of benzotriazole and fluorescent probe of coumarin, respectively. The polymeric coatings doped with the synthesized microspheres can adapt immediately to the varied pH value from corrosion electrochemical reaction and release the active molecules on demand onto the damaged cracks of coatings on metal surfaces. It leads to self-healing and self-reporting dual functions simultaneously. The pH-responsive materials with self-reporting and self-healing dual functions are highly expected to have a bright future due to their smart, long-lasting, recyclable and multifunctional properties.

Introduction

Biomimetic self-healing through adaptive repairing damages and self-reporting through registering loss of performance are two challenges in synthetic materials and are of great interest.[1] Self-healing materials have attracted increasing attentions due to their abilities of autonomous functions to protect them from damages or even to regenerate in respond to environment stress, which reduce the potential security risks and economic losses. Among the self-healing materials, capsules-based self-healing materials are capable of recovering the barrier on substrates when the materials are damaged and thereby it promotes longevityofmaterials.[2-7]For instance, White *et al*. pioneered the synthetic capsules based on self-healing coatings for anticorrosion by biomimetic strategy.[8,9]Self-healing anticorrosion coatings can delay corrosion of the metal substrates. In addition, the introduction of supramolecular dynamic chemistry into materials can develop adaptive materials such as self-healing properties in the intrinsic materials.[10-15] For instance, highly transparent polymer films with self-healing property were developed via layer-by-layer (LBL) assembly.[16,17] Binder *et al*. reported a synthetic strategy of soft-hard-soft triblock copolymers with a reversible supramolecular healing motif in the central part of the hard block.[14,18,19]

The early stages of failure or cracks of materials are inevitable and it will be beneficial to report the function loss caused by minor damage of materials. In corrosion, self-reporting of occurrence at its very early stages allows us to monitor the corrosion process and timely evaluate appropriate materials maintenance for extending the lifetime of coatings on metal surfaces. Approachto monitoring corrosion process, such as electrochemical methods,[20] electromagnetic waves,[21] infrared thermography[22], elastic wave methods[23] and pH-indicator approach[24,25]have been developed. However, the drawback of complicated instrument and premature of active molecules in coatings limited the applications of early detection of corrosion due to the minor cracks on metal surfaces.[26,27] Recently, the autonomous visual indication of mechanical damage of synthetic microcapsules encapsulated with indicator and

damage-reporting polymer materials via aggregation-induced emission have been reported.[28,29] However, there are still limited reports on self-healing and self-reporting dual functions in one material system.

In biological system, early detection and treatment in one system is highly demanding. For synthetic biomimetic materials, it is highly demanding to develop materials that possess self-reporting of early damage and self-healing simultaneously. Herein, we report a robust strategy to integrating dual functional self-healing and self-reporting of corrosion in pH-responsive polymer coatings on metals. Initially, the porous and pH-responsive polymer core-shell microspheres are synthesized for encapsulating active corrosion inhibitor of benzotriazole (BTA) and fluorescent probe of coumarin, respectively. The polymer coatings will be endowed dual functions of self-healing and self-reporting as the polymer cracks appears on metal surfaces. The polymer materials are adaptive to the environmental change, can initiate a self-healing process and will further serve as new barriers on metal surfaces to prevent further corrosion. Meanwhile, the pH-responsive polymer materials are capable of self-reporting the very early stage of corrosion due to the on demand release of fluorescent probe on minor cracks or damaged areas of polymer materials on metal surfaces.

2 Experimental Section

2.1 Materials

Divinylbenzene (DVB, 80%), 2-2'-azobisisobutyronitrile (AIBN, 99%), coumarin (99%), benzotriazole (BTA, 99%), and acrylic acid (AA, 99%) were obtained from J&K Chemical. The monomer of DVB was passed through an alkaline aluminumoxide column before use to remove the radical inhibitor. Acrylic acid was distilled under reduced pressure to remove the inhibitor and stored at 4°C before use. Recrystallization was carried out to pure azobisisobutyronitrile with anhydrous methanol. Acetonitrile (99%) and toluene (99%) were purchased from Sinopharm Chemical Reagent Company. Benzotriazole, coumarin, acetonitrile and toluenewere utilized as received without further treatment.

2.2 Synthesis of pH-Responsive and Porous PDVB-*graft*-Poly(DVB-*co*-AA) Core-Shell Microspheres by Distillation Precipitation Polymerization

The synthesis of porous PDVB-*graft*-P(DVB-*co*-AA) core-shell microspheres was carried out by distillation precipitation polymerization using toluene as porogen.[30]Typically, 10mLof DVB (total loading of monomers as 2.5 vol% of the reaction medium), 0.2 g of AIBN were dissolved in 320 mL of acetonitrile and 80 mL of toluene in a dried 500 mL two-necked flask, attached with a Liebig condenser. The reaction mixture was heated from ambient temperature to the boiling state within 20 min under slow string, and then the solvent begun to reflux. The initial homogeneous reaction mixture became milky white after boiling for 10 min. The reaction was stopped in6 h under the condition of boiling state. After the polymerization reaction, the resultant poly(divinylbenzene) (PDVB) microsphere suspension was cooled to room temperature. A varied amount of purified acrylic acid (AA, Table 1) and 2 wt% of AIBN to AA were added into the 40 mL of cooled milky suspension to copolymerized with residual DVB molecules followed by heating from room temperature to boiling state under mild stirring for another 6 h. The resulting PDVB-*graft*-(DVB-*co*-AA)core-shell microspheres were purified by repeated centrifugation, and redispersed in ethanol with ultrasonic bath for three times

followed by drying till constant weight in a vacuum oven at 50 °C.

2.3Encapsulation of Fluorescent Probe and Corrosion Inhibitor in Porous PDVB-*graft*-P(DVB-*co*-AA) Core-Shell Microspheres

To encapsulate the fluorescent probe and corrosion inhibitor in the PDVB-*graft*-P(DVB-*co*-AA) microspheres, 0.1 g of coumarin or BTA and 1 g of PDVB-*graft*-P(DVB-*co*-AA) microparticles were added into 5 mL of acetonitrile solvent followed by stirring for 24 h at 70 °C. After that, the acetonitrile in this white suspension was removed under vacuum condition with stirring at 30 °C. The resultant white powder of PDVB-*graft*-P(DVB-*co*-AA)-coumarin or PDVB-*graft*-P(DVB-*co*-AA)-BTA could be obtained after washing with50 mL of distilled water followed by drying in vacuum drying oven till a constant weight.

2.4 Polymeric Coatings with Self-Reporting and Self-Healing Dual Functions

The Q235 carbon steel plates (2 cm × 1 cm) were polished with 1000-grit sandpaper to remove any possible corrosion products, washed a few times with de-ionized water and acetone, and then dried with compressed air. The pH-responsive smart coatings were established on the metal substrates for the corrosion test. Typically, PDVB-*graft*-P(DVB-*co*-AA)-coumarin(1 wt%) and PDVB-*graft*-P(DVB-*co*-AA)-BTA (5 wt%) were mixed with Tris-(2-Hydroxyethyl)-amine harderandepoxy precursor to preparethe smart epoxy coatings. The mixture was stirred for 1 h to aid in uniform mixing. Then one treated steel coupon was dipped into the mixtures and pulled up followed by curing at 80 °C for 6 h.

The pH-triggered self-reporting and self-healing dual performances of the smart coatings was tested with a scratch inscribed by a razor. Some cracks were generated by hitting the surface of coating to have similar natural fatigue crackingon the steel panel surface. The plates were immersed in 3.5 wt% NaCl solution to accelerate the corrosion rate around the cracks. The intensity of fluorescence on the crack areas was monitored by confocal laser scanning microscopy.

2.5 Characterization

The morphology of porous PDVB-*graft*-P(DVB-*co*-AA)core-shell microspheres was characterized by Field-emission scanning electron microscopy (FESEM,JSM-7610F). The Brunauer-Emmett-Teller (BET) adsorption/desorption isotherm with nitrogen adsorption at 77K was measured with a ASAP 2020HD88 to quantify the surface area of microspheres. The UV-Vis absorption spectra of coumarin and BTA were measured at 331 nm and 275 nm, respectively, by a Labtech UV9100 double-beam spectrophotometer. The change of fluorescence intensity around the scratch area is monitored by confocal laser scanning microscopy (Zeiss LSM 710). Electrochemical impedance spectroscopy (EIS) was carried out using an electrochemical work station (CHI 660E, Shanghai Chenhua Instrument Co., Ltd, China) in a three-electrode system with a Pt foil and saturated calomel electrode (SCE) as the counter electrode and reference electrode, respectively. The EIS measurement was performedin 3.5 wt% NaCl solution with the frequency range from 10^5 Hz to 10^{-2} Hz and the amplitude of 10 mV.

3 Results and discussion

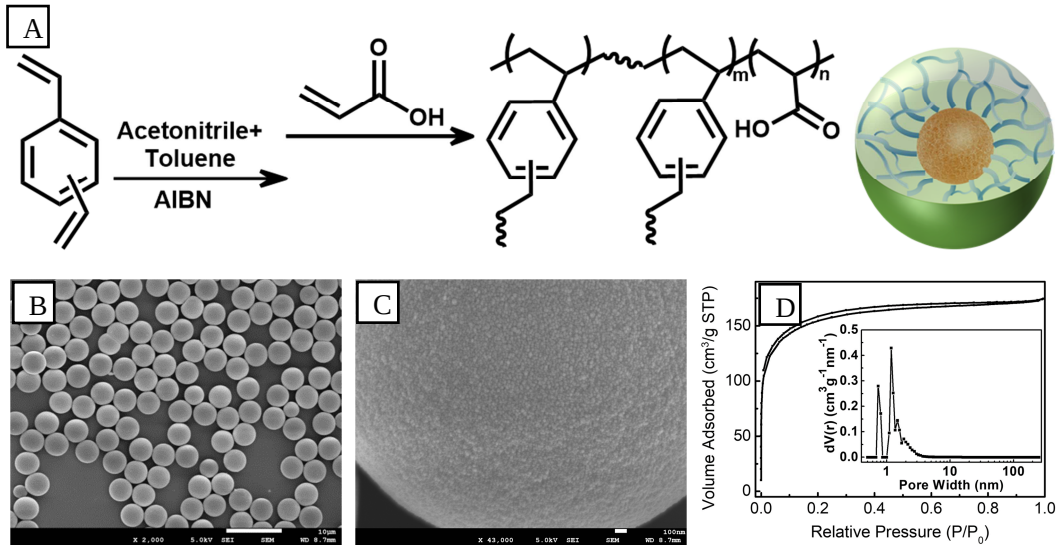

Figure 1 (a) Synthesis of pH-responsive and porous PDVB-*graft*-P(DVB-*co*-AA) core-shell microspheres; (b and c) SEM images of PDVB-*graft*-P(DVB-*co*-AA) core-shell microspheres; (d) BET data of PDVB-*graft*-P(DVB-*co*-AA) microspheres (the inset is pore size distribution calculated by DFT model).

Initially, well-defined porous PDVB-*graft*-Poly(DVB-*co*-AA) core-shell microspheres were fabricated by distillation precipitation polymerization using toluene as porogen in acetonitrile (Figure 1a).[31,32] The SEM image of resultant PDVB-*graft*-Poly(DVB-*co*-AA) microspheres are shown in Figure 1b-c. It is shown that the as-prepared polymer microspheres are with well-defined morphology. The size and size distribution of microspheres are summarized and listed in Table 1. The size of PDVB-*graft*-P(DVB-*co*-AA) core-shell microspheres can be tuned by varying the feeding amount of acrylic acid in copolymerization step, that is, the final size increases with the increased addition of monomer of acrylic acid. In contrast to the PDVB core (Entry a, Table 1), the PDVB-*graft*-Poly(DVB-*co*-AA) core-shell microspheres have an increased size, implying the successful formation of poly(DVB-*co*-AA) polymer shell on PDVB core. Furthermore, the porous PDVB-*graft*-P(DVB-*co*-AA) core-shell microspheres is characterized by the N_2-adsorption/desorption test as shown in Figure1d. The pore size distribution indicates that there are micropores (pore size < 2 nm) of as-prepared core-shell

materials. The BET surface area of porous PDVB-*graft*-P(DVB-*co*-AA) microspheres is as much as 567.8 m^2/g. The high porous nanostructure and carboxylic acid groups of resultant PDVB-*graft*-P(DVB-*co*-AA) core-shell microspheres are allowed to encapsulate active molecules and to realize pH-responsive on-demanding release for healing and indicating.

Table 1 Size and Size Distribution of Porous PDVB-*graft*-P(DVB-*co*-AA) Core-Shell Microspheres.

Entry	The amount of AA (mL)	D_n[a](μm)	D_w[a](μm)	PDI[b]
a	0	2.97	3.01	1.01
b	0.2	3.15	3.19	1.01
c	0.4	3.18	3.20	1.01

[a]$D_n(D_w)$ is the number (weight)-average data of diameter from SEM images, [b]PDI is the polydispersity index. The PDI was determined from the following statistical formula:[33]
$PDI = D_w/D_n$, $D_n = \sum_{i=1}^{k} n_i D_i / \sum_{i=1}^{k} n_i$, $D_w = \sum_{i=1}^{k} n_i D_i^4 / \sum_{i=1}^{k} n_i D_i^3$.

The fluorescent probe of coumarin and corrosion inhibitor of benzotriazole is encapsulated in pH-responsive core-shell microspheres by vacuum encapsulation, respectively (Figure 2a). FT-IR spectrum is carried out to confirm its successful encapsulation and the results are shown in Figure 2b. As shown in FT-IR spectra, the peak of 1708 cm^{-1} is attributed to the -C=O stretching band of acrylic acid segment which indicates the formation of Poly(DVB-*co*-AA) shell on the PDVB core. For the PDVB-*graft*-P(DVB-*co*-AA)-BTA, the peaks at 1209 $cm^{-1}$and 746 cm^{-1} correspond to the -N=N- vibration band and -CH bending in the aromatic ring of BTA inhibitor.[34] The peak around 1736 cm^{-1} shows a stronger absorbance which can be attributed to the -C=O stretching band of ester bond in coumarin. Anticorrosion inhibitor of BTA and fluorescent probe of coumarin have been encapsulated in microspheres successfully. Moreover, the loading amount of active healing agent and fluorescent probe can be regulated by the initial feeding ratio between active molecules and microspheres. The relationship between the loading content of coumarin and BTA encapsulated in microspheres and the initial feed content is shown in Figures 2c and 2d, respectively.

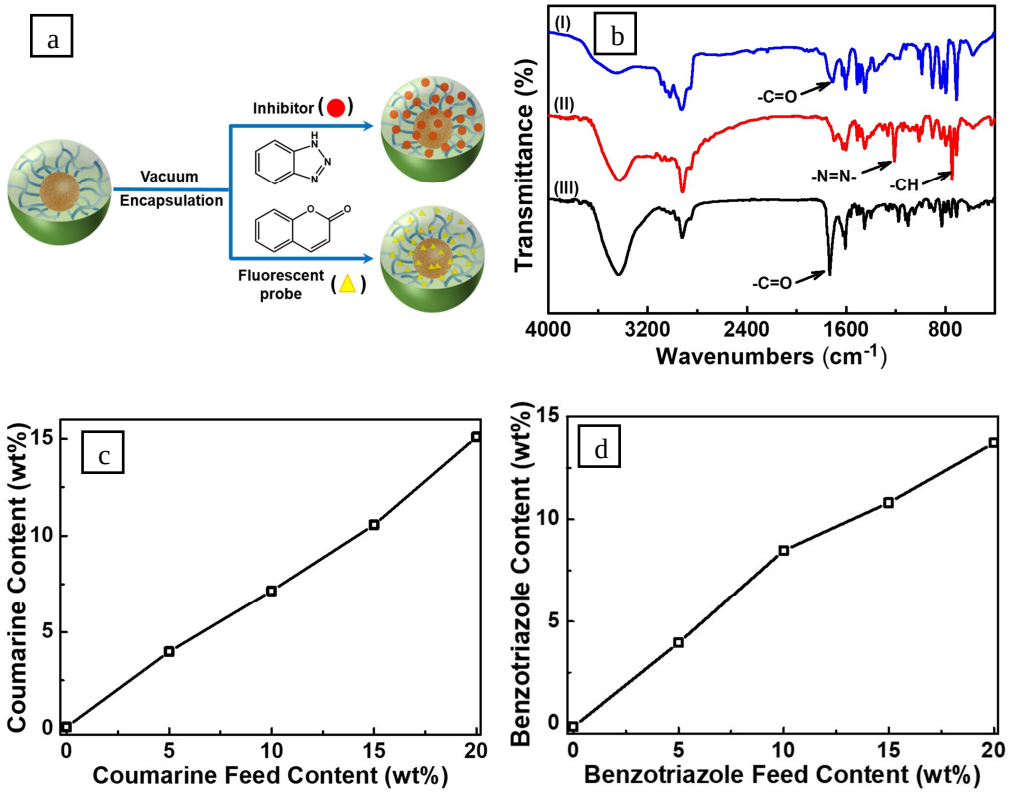

Figure 2 (a) The scheme of encapsulating anticorrosion inhibitor of benzotriazole and fluorescent probe of coumarin in PDVB-*graft*-P(DVB-*co*-AA) microspheres; (c) FT-IR spectra of PDVB-*graft*-P(DVB-*co*-AA) (I), PDVB-*graft*-P(DVB-*co*-AA)-BTA (II) and PDVB-*graft*-P(DVB-*co*-AA)-coumarin (III), respectively; (c) and (d) curves of the coumarin and BTA contents in PDVB-*graft*-P(DVB-*co*-AA) microspheres versus its feeding amount.

The pH-responsive fluorescence of PDVB-*graft*-P(DVB-*co*-AA)-coumarin is characterized by fluorescent spectroscopy and the results are shown in Figures 3a and 3b. When the pH value of solution is higher than 9, the solution exhibits a strong fluorescent intensity. We further demonstrated the controlled release dynamics of coumarin and BTA molecules from pH-responsive PDVB-*graft*-Poly(DVB-*co*-AA) microspheres in different pH solution. The release data of coumarin and BTA from pH-responsive core-shell microspheres is from by UV-Vis spectrophotometer. The release dynamics of BTA and coumarin is shown in Figures 4a and 4b. For the release dynamics of BTA from pH-responsive microspheres, the release rates within 20 min are calculated are 1.7, 3.1, 15.7 and 22.5 $\mu g \cdot mL^{-1} \cdot h^{-1}$ for pH 5, 7, 9 and 11 respectively. The release rate is getting faster as the environmental pH increases from

5 to 11. The same trend is also observed as for the release dynamics of coumarin while the release rate is 6.5, 9.4, 24.4 and 27.9 $\mu g \cdot mL^{-1} \cdot h^{-1}$ for pH value of 5, 7, 9 and 11 respectively. This is due to the pH-responsive nature of poly(DVB-*co*-AA) shell. As the pH increases, the carboxyl groups in Poly(DVB-*co*-AA) polymer shell are deprotonation which leads to the swelling of polymer chains due to electrostatic repulsion.[35] The swelling of polymer chains leads to the sustained release of BTA and coumarin molecules from microspheres. The pH-dependent sustainable release of corrosion inhibitor and fluorescent molecules from well-defined morphological PDVB-*graft*-P(DVB-*co*-AA) microspheres suggests that the as-prepared PDVB-*graft*-P(DVB-*co*-AA)-BTA and PDVB-*graft*-P(DVB-*co*-AA)-coumarin can serve as a good candidate for self-healing and self-reporting multifunctional coatings on metal surfaces.

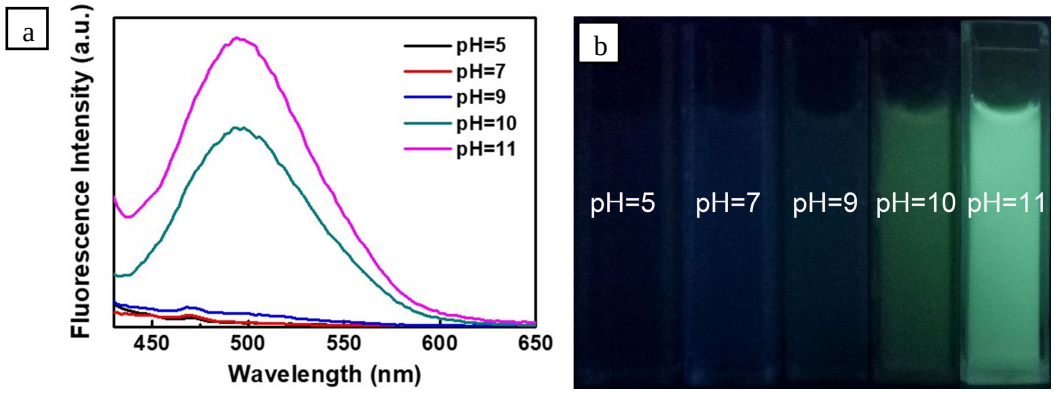

Figure 3 (a) The fluorescence intensity by fluorescent spectroscopy of PDVB-*graft*-P(DVB-*co*-AA)-coumarin in different pH solutions (40 μg/mL of coumarin); (b) Optical graphs of PDVB-*graft*-P(DVB-*co*-AA)-coumarin by 365 nm UV lamp in different pH solutions (40 μg/mL of coumarin).

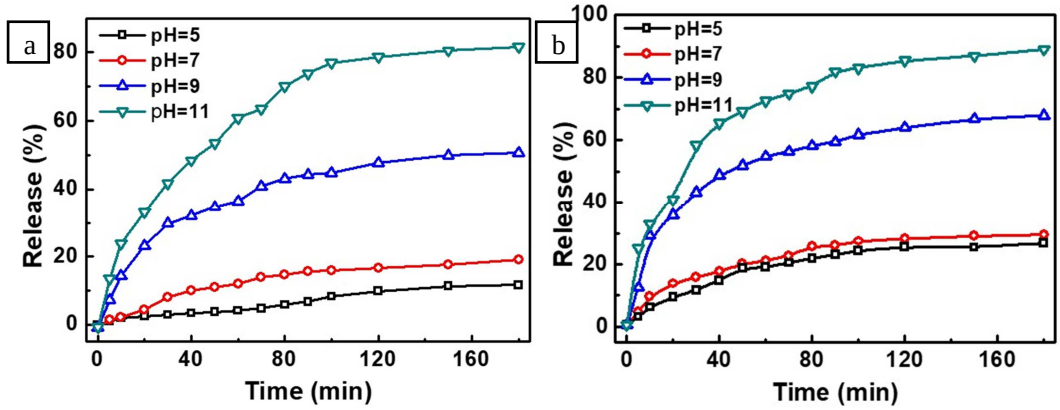

Figure 4 Release dynamics of benzotriazole (a) and coumarin (b) from pH-responsive PDVB-*graft*-P(DVB-*co*-AA) core-shell microspheres in different pH solution.

The pH-responsive polymer coatings with autonomous self-reporting and self-healing dual functions are constructed by doping PDVB-*graft*-P(DVB-*co*-AA)-coumarin and PDVB-*graft*-P(DVB-*co*-AA)-BTA microspheres into epoxy resins. The fluorescent intensity is monitored by confocal laser scanning microscopy with excitation wavelength λ_{ex}= 405 nm (Figures 5a and 5b). The coatings can respond to pH change during corrosion electrochemical reaction. The fluorescence under the condition of pH 11 implies that there is uniform dispersion of microspheres in epoxy coatings (Figure 5b). The direct addition of fluorescent probes into polymer coatings can detect steel corrosion. However, the severe problem of premature fluorescence limited their further application.[36,37] Herein, the fluorescent probe of coumarin are encapsulated in the as-prepared PDVB@P(DVB-*co*-AA) core-shell microspheres, thus avoiding any premature before it is triggered by high pH from electrochemical reaction. When scratch was made and confocal photographs were taken before and after the samples immersed in 3.5 wt% NaCl solution for 6 h. As shown in Figures 5d and 5e, there is no fluorescence at the initial stage, while very distinctive fluorescence appears round the cracks of polymer coatings after immersion in salts. It is hard to notice the corrosion occurrence from the photographs. However, it is shown that there is high efficiency of pH-responsive epoxy coating for self-reporting of corrosion at the very early stage. We further demonstrate the self-reporting ability to fatigue cracking mimicked by hammering the pH-responsive polymer coating. The fluorescence indication along the cracks can be monitored clearly (Figure 5g). In contrast, it is hard to notice that corrosion already occurs in optical image (Figure 5f). These results above suggest that pH-responsive polymer coating can provide a new non-destructive method for reporting early stages of metal corrosion.

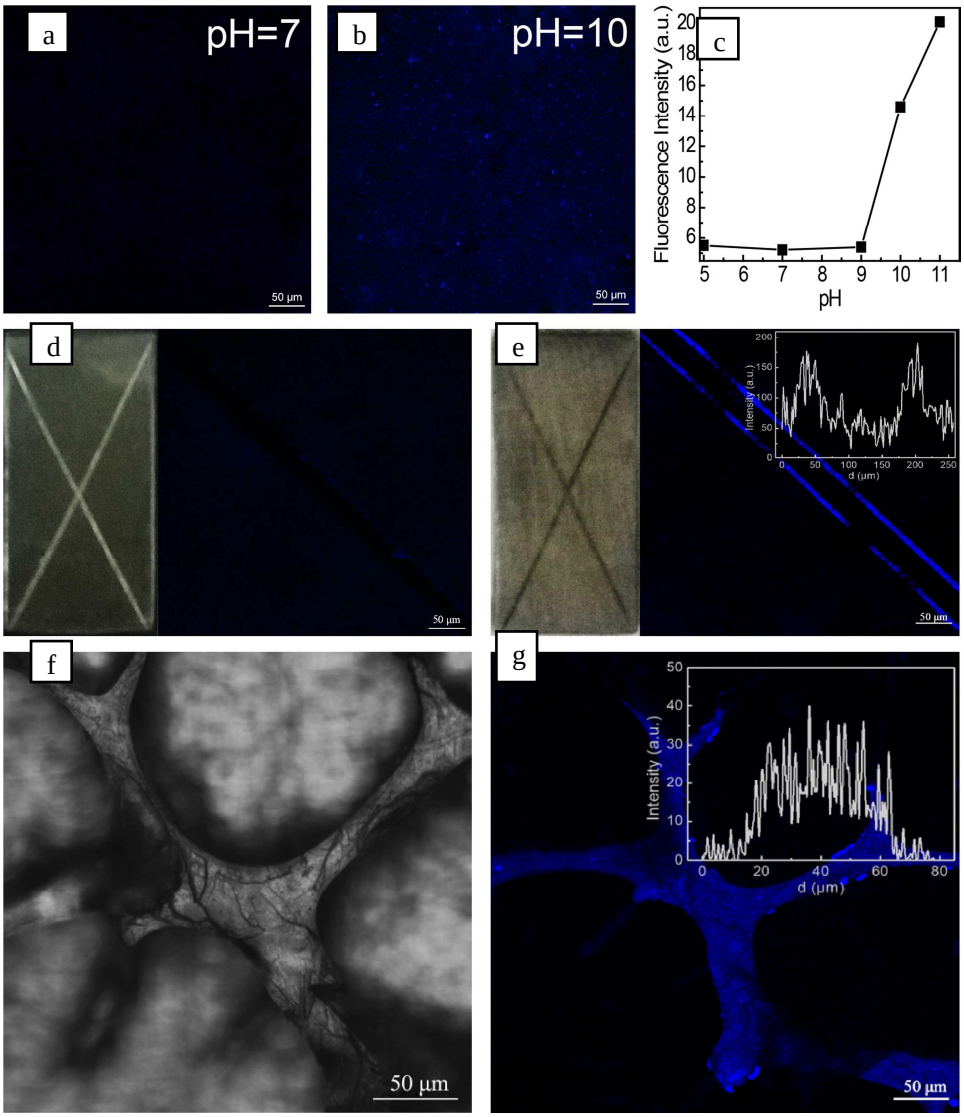

Figure 5 Confocal laser scanning microscopy of pH-responsive coatings after immersion in different pH solution for 48 h (a and b); (c) Mean fluorescence intensity of pH-responsive coatings in different pH solutions; Confocal laser scanning microscopy of the scratched area before (d) and after (e) immersion in 3.5 wt% NaCl solution for 6 h; Digital camera image (f) and confocal image (g) of the cracking after immersed in 3.5 wt% NaCl solution for 6 h; The insets in (e) and (g) are fluorescent intensity with the displacement perpendicular to the crack of polymer coatings.

The self-healing anticorrosion performance of the pH-responsive epoxy coatings is further demonstrated. Scratch corrosion tests were performed on carbon steels in Figure 6a. The as-prepared pH-responsive coatings doped with PDVB-*co*-P(DVB-*co*-AA) core-shell microspheres displayed an improved anticorrosion protection on the crack area in contrast to the pure polymer coatings. There is almost no corrosion propagation, implying that the electrochemical corrosion

has been inhibited. Remarkably, after one month in 3.5 wt% NaCl solution, the sample with pH responsive coatings has no obvious corrosion production while the sample without smart coatings was corroded seriously, which indicates the long-term anticorrosion effects of the dual-functionalized smart coatings (Supporting Information, Figure S4). We utilize EIS to evaluate the anticorrosion performance of the coatings. The evolutions of Bode plots and Nyquist plots with immersion time for the pure epoxy coating and the pH-responsive epoxy coating are shown in Figures 6b, 6c, respectively. In general, $|Z|_{0.01\ Hz}$, the impedance modulus at the lowest frequency represents the barrier performance of the coatings. At the beginning of immersion, the Bode plots of these two coatings have nearly no difference. With the extension of immersion time, the aggressive electrolyte species (e.g., Cl^-) would penetrate into the pores of the coatings and then reach to the surface of the substrate metals, causing the decrease of the impedance modulus of the coatings. In Figure 6b, $|Z|_{0.01\ Hz}$ of the pure epoxy coating reduces obviously from $3.27 \times 10^8 \Omega\ cm^2$ to $2.58 \times 10^7\ M\Omega\ cm^2$ after the immersion of 96 h, indicating the deterioration of the barrier effect of the coatings with time. However, for pH-responsive epoxy coating, $|Z|_{0.01\ Hz}$ exhibits a slight drop from $2.60 \times 10^8 \Omega\ cm^2$ to $1.76 \times 10^8 \Omega\ cm^2$, which suggests its good anticorrosion performance for the substrate metal. Moreover, as shown in Figure 6c, the larger capacitive arcs in Nyquist plots can also prove the better barrier function of the pH-responsive epoxy coating. The EIS results can be further fitted using an equivalent circuit in Figure 6d. The equivalent circuit is defined as $R_s(C_{coat}(R_{coat}(Q_{dl}R_{ct})))$ in which R_s, C_{coat}, R_{coat}, Q_{dl} and R_{ct} represent solution resistance, coating capacitance, coating resistance, constant phase element and charge transfer resistance, respectively. The fitting results using the equivalent circuit including R_{coat} and C_{coat} are shown in Figures 6e and 6f. R_{coat} means the resistance to aggressive species transfer through the coatings and C_{coat} reflects the water uptake tendency of the coatings.[38] Therefore, the coatings with good anticorrosion performance possess high R_{coat} value and low C_{coat} value. After the samples was immersed with 96 h, the R_{coat} of the pure epoxy coating gradually decreases from $2.67 \times 10^6\ \Omega\ cm^2$ to $1.26 \times 10^5 \Omega\ cm^2$ and the C_{coat}

increases from 1.05×10^{-12} F cm^{-2} to 2.79×10^{-10} F cm^{-2}, which indicates the decrease in anticorrosion ability. For comparison, the R_{coat} of the pH responsive coating keeps much higher values (from 2.78×10^{6} Ω cm^2 to 1.50×10^{6} Ω cm^2) and the C_{coat} maintains lower values (from 1.18×10^{-12} F cm^{-2} to 2.01×10^{-12} F cm^{-2}). Therefore, the pH responsive coating can provide good anticorrosion property for the substrate metal.

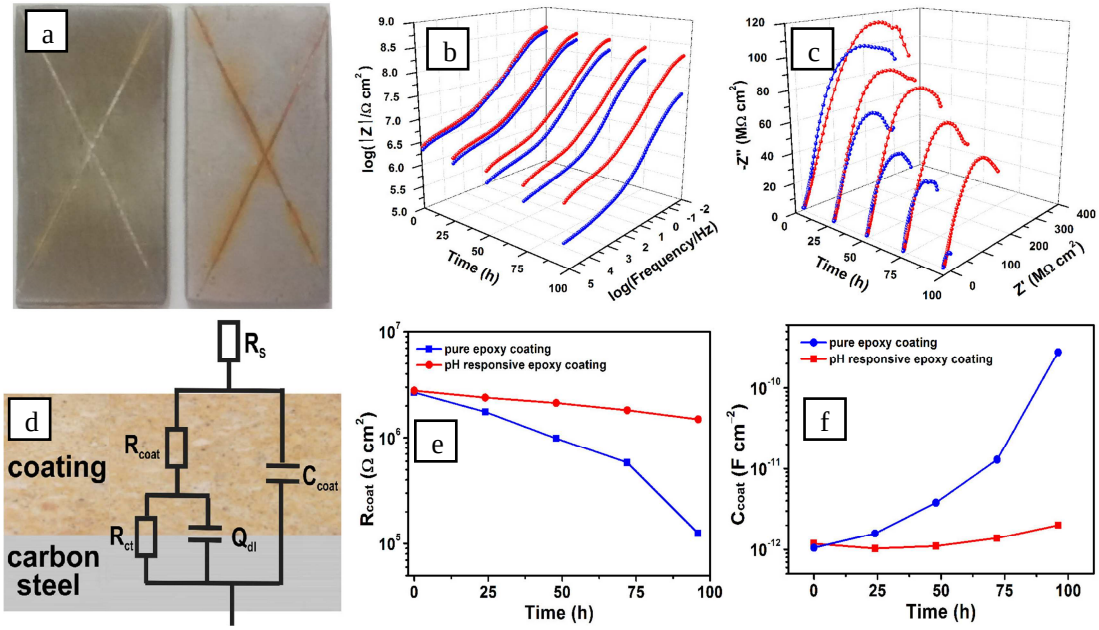

Figure 6 (a) Self-healing anticorrosion performance of pH-responsive coating on surface of carbon steel for 6 h in NaCl solution; Bode plots (b) and Nyquist plots (c) of the carbon steel coated with the pure epoxy coating (blue) and pH-responsive epoxy coating (red) in 3.5 wt% NaCl solution; (d) Schematic diagram of the equivalent circuit model; (e-f) Evolution of R_{coat} and C_{coat} with immersion time obtained by the EIS results using the equivalent circuit. The left (or right) in image of (a) is with (or without) 1 wt% of PDVB-*graft*-P(DVB-*co*-AA)-coumarin and 5 wt% of PDVB-*graft*-P(DVB-*co*-AA)-BTA microspheres in epoxy coatings.

The mechanism of self-reporting of corrosion at the early stage and self-healing of the pH-responsive polymer coating for protection is illustrated in Figure 7. Once the coatings on steel surfaces are scratched, the coating cannot serve as a passive barrier any more to repel corrosive species away from contacting with the steel. Thus, the carbon steel surfaces are more susceptible to fast corrosion expansion. When metal surfaces are exposed to corrosive species such as oxygen, water, and chloride ions, a typical galvanic cell will be established and the anode and cathode reactions are as

follows:[39,40]

$$\text{Anode: } 2\ Fe \rightarrow 2\ Fe^{2+} + 4\ e^{-} \quad (1)$$

$$\text{Cathode: } O_2 + 2\ H_2O + 4\ e^{-} \rightarrow 4\ OH^{-} \quad (2)$$

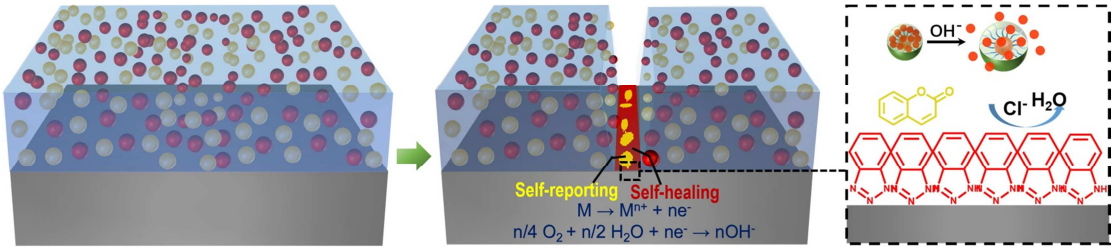

Figure 7 The mechanism for pH-responsive polymer coatings with self-reporting for early detection of corrosion and self-healing dual functions.

The iron atoms incline to lose valence electrons while oxygen obtain the electrons to yield OH^-. The pH-responsive microspheres can respond to the increased pH around the crack areas caused by initiation of electrochemical corrosion process. The quick release of fluorescent probe of coumarin and corrosion inhibitor of BTA on the scrached areas, thus allowing fast fluorescence imaging/indication of early corrosion and suppressing corrosion to restore coating functionality. Finally, a complete antonomous life-cycle control is realized. Remarkably, the construction of smart coatings with self-reporting and self-healing dual functions developed cam serve as general approach for other metals such as copper, magnesium, and aluminium alloys.. Compared with pure epoxy coatings, the smart coatings in Figure 8 exhibited self-healing for anticorrosion and self-reporting for early detection of corrosion to enhance the material service life and reduce the risk of accidents.

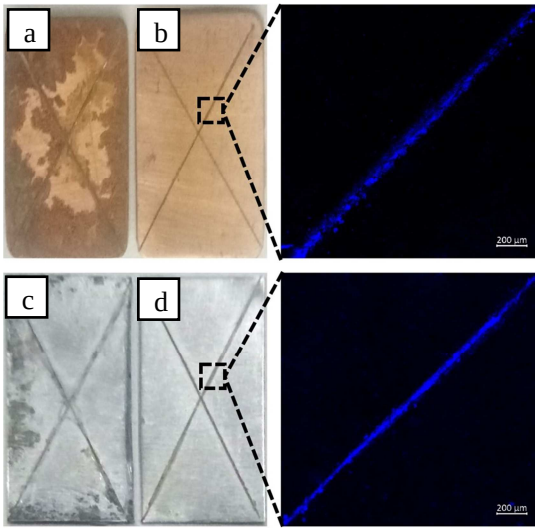

Figure 8 Smart polymer coatings doped with (b and d) and without (control samples, a and c) 1 wt% of PDVB-*graft*-P(DVB-*co*-AA)-coumarin and 5 wt% of PDVB-*graft*-P(DVB-*co*-AA)-BTA microspheres to have self-reporting and self-healing dual functions on copper alloy and aluminium alloy surfaces in 3.5 wt% NaCl solution for 6 h.

4 Conclusions

Integration of self-reporting and self-healing performance in polymer coatings based on pH-responsive and porous PDVB-*graft*-P(DVB-*co*-AA) core-shell microspheres have been demonstrated. The efficient synthesis of porous and pH-responsive polymer microspheres with well-defined morphology provides strategy for construction of pH-responsive polymeric coatings on metal surfaces. The fluorescence of coumarin and corrosion inhibition of BTA encapsulated in PDVB-*graft*-P(DVB-*co*-AA) core-shell microspheres are under dormant state when the polymer coatings on metals are in well state. Triggered by increased pH value by corrosion reactions around the crack or damaged areas of polymeric coatings on metal surfaces, the fluorescence of coumarin can be active and indicate for reporting early stages of corrosion on time. Meanwhile the BTA healing molecules reserve as dense barriers on metal surface simultaneously. The polymer materials with self-reporting and self-healing dual functions meet the future demands of long lasting of lifetime of synthetic materials and one may expect for it a bright future.

Acknowledgement

G. Li acknowledges support by the One Hundred Talent Program of Chinese Academy of Sciences and National Key Research and Development Plan (Grant No. 2016YFC0303700).

Supporting Information

The supporting information is available free of charge on the ACS Publication website. FTIR Spectra of PDVB-*graft*-P(DVB-*co*-AA) core-shell microspheres, the standard curve of benzotriazole and coumarin in 0.2 mol/L NaOH solution at 275 nm and 331 nm respectively, and the optical images of coating samples and controlled pure epoxy coating after being immersed in 3.5 wt% NaCl solution.

The authors declare no competing financial interest.

References and Notes

(1) Patrick, J. F.; Robb, M. J.; Sottos, N. R.; Moore, J. S.; White, S. R. *Nature* **2016**, *540*, 363.

(2) White, S. R.; Sottos, N. R.; Geubelle, P. H.; Moore, J. S.; Kessler, M. R.; Sriram, S. R.; Brown, E. N.; Viswanathan, S. *Nature* **2001**, *409*, 794.

(3) Tran, T. H.; Vimalanandan, A.; Genchev, G.; Fickert, J.; Landfester, K.; Crespy, D.; Rohwerder, M. *Adv. Mater.* **2015**, *27*, 3825.

(4) Lv, L. P.; Zhao, Y.; Vilbrandt, N.; Gallei, M.; Vimalanandan, A.; Rohwerder, M.; Landfester, K.; Crespy, D. *J. Am. Chem. Soc*. **2013**, *135*, 14198.

(5) Fickert, J.; Makowski, M.; Kappl, M.; Landfester, K.; Crespy, D. *Macromolecules* **2012**, *45*, 6324.

(6) Haase, M. F.; Grigoriev, D. O.; Mohwald, H.; Shchukin, D. G. *Adv. Mater.* **2012**, *24*, 2429.

(7) Abdullayev, E.; Abbasov, V.; Tursunbayeva, A.; Portnov, V.; Ibrahimov, H.; Mukhtarova, G.; Lvov, Y. *ACS Appl. Mater. Inter.* **2013**, *5*, 4464.

(8) Diesendruck, C. E.; Sottos, N. R.; Moore, J. S.; White, S. R. *Angew. Chem. Int. Ed.* **2015**, *54*, 10428.

(9) Cho, S. H.; Andersson, H. M.; White, S. R.; Sottos, N. R.; Braun, P. V. *Adv. Mater.* **2006**, *18*, 997.

(10) Studart, A. R. *Angew. Chem. Int. Ed.* **2015**, *54*, 3400.

(11) Yang, L. L.; Tan, X. X.; Wang, Z. Q.; Zhang, X. *Chemical Reviews* **2015**, *115*, 7196.

(12) Neuser, S.; Chen, P. W.; Studart, A. R.; Michaud, V. *Advanced Engineering Materials* **2014**, *16*, 581.

(13) Xiong, Y. B.; Chen, Z. J.; Wang, H.; Ackermann, L. M.; Klapper, M.; Butt, H. J.; Wu, S. *Chem. Commun.* **2016**, *52*, 14157.

(14) Chen, S. B.; Mahmood, N.; Beiner, M.; Binder, W. H. *Angew. Chem. Int. Ed.* **2015**, *54*, 10188.

(15) Zhang, M. M.; Xu, D. H.; Yan, X. Z.; Chen, J. Z.; Dong, S. Y.; Zheng, B.; Huang, F. H. *Angew. Chem. Int. Ed.* **2012**, *51*, 7011.

(16) Li, Y.; Chen, S. S.; Li, X.; Wu, M. C.; Sun, J. Q. *Acs Nano* **2015**, *9*, 10055.

(17) Li, Y. X.; Fang, X.; Wang, Y.; Ma, B. H.; Sun, J. Q. *Chem. Mater.* **2016**, *28*, 6975.

(18) Enke, M.; Dohler, D.; Bode, S.; Binder, W. H.; Hager, M. D.; Schubert, U. S. *Adv. Polym. Sci.* **2016**, *273*, 59.

(19) Dohler, D.; Peterlik, H.; Binder, W. H. *Polymer* **2015**, *69*, 264.

(20) Andrade, C.; Keddam, M.; Novoa, X. R.; Perez, M. C.; Rangel, C. M.; Takenouti, H. *Electrochim. Acta* **2001**, *46*, 3905.

(21) Sbartaï, Z. M.; Laurens, S.; Rhazi, J.; Balayssac, J. P.; Arliguie, G. *J Appl. Geophys.* **2007**, *62*, 361.

(22) Bagavathiappan, S.; Lahiri, B. B.; Saravanan, T.; Philip, J.; Jayakumar, T. *Infrared Phys. Techn.* **2013**, *60*, 35.

(23) Sohn, H.; Park, G.; Wait, J. R.; Limback, N. P.; Farrar, C. R. *Smart Mater. Struct.* **2004**, *13*, 153.

(24) Maia, F.; Tedim, J.; Bastos, A. C.; Ferreira, M. G. S.; Zheludkevich, M. L. *RSC Adv.* **2014**, *4*, 17780.

(25) Augustyniak, A.; Ming, W. *Prog. Org. Coat.* **2011**, *71*, 406.

(26) Augustyniak, A.; Tsavalas, J.; Ming, W. *ACS Appl. Mater. Inter.* **2009**, *1*, 2618.

(27) Li, W.; Matthews, C. C.; Yang, K.; Odarczenko, M. T.; White, S. R.; Sottos, N. R. *Adv. Mater.* **2016**, *28*, 2189.

(28) Li, W. L.; Matthews, C. C.; Yang, K.; Odarczenko, M. T.; White, S. R.; Sottos, N. R. *Adv Mater* **2016**, *28*, 2189.

(29) Robb, M. J.; Li, W.; Gergely, R. C. R.; Matthews, C. C.; White, S. R.; Sottos, N. R.; Moore, J. S. *Acs Central Sci* **2016**, *2*, 598.

(30) Bai, F.; Huang, B.; Yang, X.; Huang, W. *Polymer* **2007**, *48*, 3641.

(31) Bai, F.; Huang, B.; Yang, X. L.; Huang, W. Q. *Polymer* **2007**, *48*, 3641.

(32) Bai, F.; Yang, X. L.; Li, R.; Huang, B.; Huang, W. Q. *Polymer* **2006**, *47*, 5775.

(33) Li, G. L.; Wan, D.; Neoh, K. G.; Kang, E. T. *Macromolecules* **2010**, *43*, 10275.

(34) Miao, M.; Yuan, X.-Y.; Wang, X.-G.; Lu, Y.; Liu, J.-K. *Dyes and Pigments* **2017**, *141*, 74.

(35) Li, G. L.; Liu, G.; Kang, E. T.; Neoh, K. G.; Yang, X. L. *Langmuir* **2008**, *24*, 9050.

(36) Johnson, R. E.; Agarwala, V. S. *Mater Performance* **1994**, *33*, 25.

(37) Augustyniak, A.; Tsavalas, J.; Ming, W. H. *Acs Appl Mater Inter* **2009**, *1*, 2618.

(38) Wang, M.; Liu, M.; Fu, J. *J Mater. Chem. A* **2015**, *3*, 6423.

(39) Shchukin, D. G.; Zheludkevich, M.; Yasakau, K.; Lamaka, S.; Ferreira, M. G. S.; Möhwald, H. *Adv. Mater.* **2006**, *18*, 1672.

(40) Hughes, A. E.; Cole, I. S.; Muster, T. H.; Varley, R. J. *NPG Asia Mater.* **2010**, *2*, 143.